BIOCHEMISTRY
including biophysical chemistry & molecular biology

Article

pubs.acs.org/biochemistry

Crystal Structure and Product Analysis of an Archaeal *myo*-Inositol Kinase Reveal Substrate Recognition Mode and 3-OH Phosphorylation

Ryuhei Nagata,[†] Masahiro Fujihashi,[†] Takaaki Sato,[‡,§] Haruyuki Atomi,[‡,§] and Kunio Miki*[,†,§]

[†]Department of Chemistry, Graduate School of Science, Kyoto University, Sakyo-ku, Kyoto 606-8502, Japan

[‡]Department of Synthetic Chemistry and Biological Chemistry, Graduate School of Engineering, Kyoto University, Katsura, Nishikyo-ku, Kyoto 615-8510, Japan

[§]JST, CREST, 7, Gobancho, Chiyoda-ku, Tokyo 102-0076, Japan

Supporting Information

ABSTRACT: The TK2285 protein from *Thermococcus kodakarensis* was recently characterized as an enzyme catalyzing the phosphorylation of *myo*-inositol. Only two *myo*-inositol kinases have been identified so far, the TK2285 protein and Lpa3 from *Zea mays*, both of which belong to the ribokinase family. In either case, which of the six hydroxyl groups of *myo*-inositol is phosphorylated is still unknown. In addition, little is known about the *myo*-inositol binding mechanism of these enzymes. In this work, we determined two crystal structures: those of the TK2285 protein complexed with the substrates (ATP analogue and *myo*-inositol) or the reaction products formed by the enzyme. Analysis of the ternary substrates-complex structure and site-directed mutagenesis showed that five residues were involved in the interaction with *myo*-inositol. Structural comparison with other ribokinase family enzymes indicated that two of the five residues, Q136 and R140, are characteristic of *myo*-inositol kinase. The crystal structure of the ternary products-complex, which was prepared by incubating the TK2285 protein with *myo*-inositol and ATP, holds 1D-*myo*-inositol 3-phosphate (Ins(3)P) in the active site. NMR and HPLC analyses with a chiral column also indicated that the TK2285 reaction product was Ins(3)P. The results obtained here showed that the TK2285 protein specifically catalyzes the phosphorylation of the 3-OH of *myo*-inositol. We thus designated TK2285 as *myo*-inositol 3-kinase (MI3K). The precise identification of the reaction product should provide a sound basis to further explore inositol metabolism in Archaea.

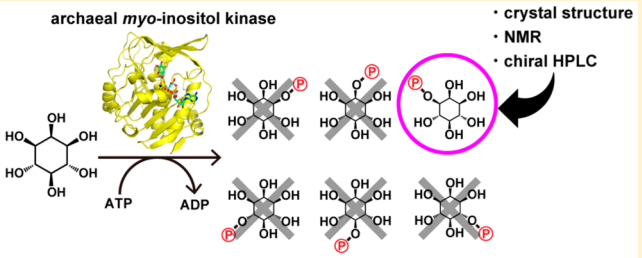

Sugars are metabolized to sugar phosphates in cells. Phosphorylation of glucose is known to be the first step in the Embden−Meyerhof pathway for all three domains of life.[1] Many sugar kinases have been isolated and classified into three families (the hexokinase family, ribokinase family, and galactokinase family) based on their primary and tertiary structures.[2] Each family contains various kinases. For example, the ribokinase family consists of a wide range of enzymes including ribokinase, adenosine kinase, and tagatose 6-phosphate kinase. (for a review, see ref 3).

TK2285 is an enzyme from the hyperthermophilic archaeon *Thermococcus kodakarensis* and belongs to the ribokinase family.[4] We have reported the prominent phosphorylation activity of this enzyme toward *myo*-inositol.[4] To date, only two *myo*-inositol kinases have been identified. One is the TK2285, and the other is Lpa3 from a crop plant, *Zea mays*.[5] Both of these enzymes belong to the ribokinase family (sequence identity: 22%) and transfer a phosphate from ATP to *myo*-inositol to produce *myo*-inositol monophosphate(s) and ADP.[4,5] However, which of the six hydroxyl groups of *myo*-inositol is phosphorylated is still unknown, as the enantiomerism of the *myo*-inositol monophosphates makes identification of the phosphorylation position difficult. Gas chromatography/mass spectrometry analysis showed that the Lpa3 products are composed of *myo*-inositol 1/3-phosphate, *myo*-inositol 4/6-phosphate, and/or possibly *myo*-inositol 5-phosphate[5] (unless specified, the atom nomenclature of *myo*-inositol corresponds to 1D-*myo*-inositol[6−8]). However, the analysis of the Lpa3 reaction products distinguishing between *myo*-inositol 1- and 3-phosphate or between *myo*-inositol 4- and 6-phosphate (i.e., enantiomeric identification) has not been performed. Therefore, identification of the products of *myo*-inositol kinase would greatly promote our understanding of inositol metabolism.

Until now, the only crystal structure determined for *myo*-inositol kinase is the unliganded structure of TK2285.[4] This enzyme is a monomeric enzyme with an approximate molecular weight of 30,300. The overall structure of TK2285 resembles the structures of other ribokinase family members that consist

Received: March 18, 2015
Revised: May 2, 2015
Published: May 14, 2015

DOI: 10.1021/acs.biochem.5b00296
Biochemistry 2015, 54, 3494−3503

of a large $\alpha\beta\alpha$ domain and a small lid domain, and the TK2285 active site is considered to be located between the two domains.[2,4] Two characteristic features of ribokinases around the ligand-binding site are also observed in the TK2285 protein.[4] The first one is a glycine-rich motif, which induces a lid domain motion to close the active site via substrate binding. The other is the catalytic aspartate, which is thought to activate the hydroxyl group of the phosphate acceptor and corresponds to D219 in TK2285. However, much about TK2285 remains to be elucidated, particularly the details of the binding mode between this enzyme and *myo*-inositol.

In this work, we determined the crystal structures of two ternary complexes, one between the TK2285 protein and substrates and the other between the TK2885 protein and products. The structure analysis of the ternary products-complex and analyses of the reaction product by NMR and HPLC with a chiral column demonstrated that the phosphorylated product of *myo*-inositol kinase is 1D-*myo*-inositol 3-phosphate (Ins(3)P). We therefore named this enzyme *myo*-inositol 3-kinase, which we abbreviate as MI3K. The ternary substrates-complex structure revealed the substrate-recognition mode of this enzyme. Site-directed mutagenesis and structural comparison with MI3K homologues identified the characteristic residues for *myo*-inositol kinases.

MATERIALS AND METHODS

Site-Directed Mutagenesis. Plasmids for the expression of TK2285 mutants (D12A, Q136A, and R140A) were prepared by inverse polymerase chain reaction (PCR). pET21a-TK2285[4] and the following oligonucleotides were used as a template DNA and primers, respectively: D12A-F/D12A-R {5′-GTTGTCAGGGCCATAGTTAAAAAAGGCAACAAG-3′/5′-CTATGCCCCTGACAACATGGCCAACAACAAG-3′}, Q136A-F/Q136A-R {5′-GGTTGACATAGCGGGGTTTATCCGTTCCTCAAG-3′/5′-GGATAAACCCCGCTATGTCAACCGCAACAACTGG-3′}, and R140A-F/R140A-R {5′-GGGTTTATCGCTTCCTCAAGTCCAGGAGAAATTC-3′/5′-CTTGAGGAAGCGATAAACCCCTGTATGTCAACC-3′}. The sequences of the resulting mutant plasmids were confirmed by DNA sequencing (Hokkaido System Science Co. Ltd., Sapporo, Japan).

Expression and Purification of TK2285 and Its Mutants. *Escherichia coli* strain Rosetta2(DE3)pLysS was used for expressing wild-type TK2285 and its mutants. The cells were transformed by the plasmid pET21a-TK2285 or the plasmids for the mutants described above. The transformants were cultured at 37 °C in Luria−Bertani medium containing 50 μg/mL carbenicillin and 45 μg/mL chloramphenicol. At a cell density of 0.4 (optical density at 600 nm), isopropyl-1-thio-D-galactopyranoside (final 0.1 mM) was added to induce gene expression. After a further culture for 4 h, the cells were harvested by centrifugation (5,000*g*, 20 min, 4 °C).

The cells were resuspended in Buffer A (50 mM Tris-HCl (pH 7.5) and 1 mM dithiothreitol (DTT)) containing an EDTA-free protease inhibitor cocktail (Nacalai Tesque, Kyoto, Japan) and disrupted by sonication. After adding DTT (final 10 mM), the sonicate was treated at 85 °C for 30 min and centrifuged (20,000*g*, 30 min, 4 °C). The supernatant was applied to a 6 mL Resource Q column (GE Healthcare, Little Chalfont, UK) equilibrated with Buffer A and eluted with a gradient of 0 to 1 M NaCl. The eluted fractions at NaCl concentrations of 50−150 mM were mixed with an equal volume of Buffer A containing 3 M $(NH_4)_2SO_4$, and applied to a 6 mL Resource PHE column (GE Healthcare) equilibrated with Buffer B (50 mM Tris-HCl (pH 7.5), 1 mM DTT, and 1.5 M $(NH_4)_2SO_4$). The TK2285 protein was eluted at $(NH_4)_2SO_4$ concentrations of 1.35−1.12 M by a gradient of 1.5 to 0 M $(NH_4)_2SO_4$. The buffer of the fractions including TK2285 was exchanged with Buffer A by using an ultrafiltration column. The sample was used for the kinase-activity measurement. For the crystallization, the sample was additionally applied to a 0.8 mL Mini Q column (GE Healthcare) equilibrated with Buffer A. The elution was performed with a gradient of 0 to 100 mM NaCl. The eluted sample at NaCl concentrations of 26−47 mM appeared to be homogeneous in both SDS- and native-polyacrylamide gel electrophoresis (PAGE).

Crystallization. Crystallization was performed with the sitting-drop vapor diffusion method at 20 °C. The protein concentration was determined by the UV absorbance at 280 nm with the extinction coefficient (20400 M^{-1} cm^{-1}) calculated by the program ProtParam.[9]

The purified TK2285 protein was crystallized as the ternary substrates-complex and the ternary products-complex. For crystallization of the ternary substrates-complex, 10 mg/mL of the TK2285 protein with 10 mM β,γ-methyleneadenosine 5′-triphosphate (AMP-PCP), 10 mM *myo*-inositol, and 10 mM $MgCl_2$ in a buffer of 100 mM Tris-HCl (pH 7.5) and 10 mM DTT was treated at 85 °C for 30 min and filtered using a 0.22 μm pore size filter. For crystallization of the ternary products-complex, 10 mg/mL of the TK2285 protein was mixed with 10 mM ATP, 10 mM *myo*-inositol, and 10 mM $MgCl_2$ in Buffer A. The mixture was incubated at 85 °C for 5 min in order to convert the substrates into the products. DTT was then added to a final concentration of 10 mM and heat-treated again at 85 °C for 30 min as with the previous work.[4] The crystallization was performed using the filtered sample from the heat-treated mixture. Each solution for the crystallization was blended with an equal amount of the precipitant solution composed of 14−20% (w/v) polyethylene glycol 3350 and 0.2 M NH_4I and equilibrated at 20 °C against the same precipitant solution. Crystals were typically obtained within 3 to 7 days.

Data Collection and Model Refinement. The crystals were soaked in a cryo-protectant solution composed of 16% (w/v) polyethylene glycol 3350, 0.2 M NH_4I, and 20% (v/v) ethylene glycol for a few seconds and flash-frozen in a nitrogen stream at 95 K. Diffraction data sets were collected at the beamline NE3A of the Photon Factory Advanced Ring. The data sets were integrated and scaled with the program HKL2000.[10] The phases were determined by Fourier synthesis using the unliganded structure of TK2285 (Protein Data Bank (PDB) ID: 3W4S[4]) as the starting model. The structures were constructed using the program COOT[11] and refined using the program REFMAC5[12,13] with the Translation Libration Screw refinement technique. The diffraction data set was truncated at the resolution whose R_{sym} of the shell is ∼0.3. The refined models of the ternary substrates-complex structure and the ternary products-complex structure were composed of 22 and 17 iodine anions with the occupancies of 1.0−0.2 and 1.0−0.3, respectively, derived from the precipitant solution, but they were not observed at the ligand-binding site.

In the model of the ternary products-complex, the electron density corresponding to the phosphate part of Ins(3)P was relatively weak. Therefore, Ins(3)P and *myo*-inositol were assigned occupancies of 70% and 30%, respectively, based on the electron density and the temperature factor of their refined structures. No significant peaks are found around Ins(3)P in

DOI: 10.1021/acs.biochem.5b00296
Biochemistry 2015, 54, 3494−3503

Table 1. Data Collection and Refinement Statistics

	ternary substrates-complex	ternary products-complex
	Data collection	
X-ray source	Photon Factory Advanced Ring NE3A	Photon Factory Advanced Ring NE3A
wavelength (Å)	1.0000	1.0000
space group	$P2_12_12_1$	$P2_12_12_1$
cell parameters ($a/b/c$ (Å))	77.1/81.2/81.1	77.4/81.3/82.0
resolution (Å)[a]	50−1.93 (1.96−1.93)	50−2.08 (2.12−2.08)
no. of obs. reflections	277594	217977
no. of unique reflections	38880	31830
redundancy	7.1	6.8
completeness (%)[a]	99.7 (100)	99.7 (100)
$I/\sigma(I)$[a]	26.3 (7.0)	21.5 (6.8)
R_{sym} (%)[a,b]	7.2 (29.8)	8.0 (29.7)
	Refinement	
resolution (Å)	50−1.93	50−2.08
R/R_{free} (%)[c]	21.59/25.46	20.29/25.02
no. of atoms (protein/ligand/solvent[d])	4165/88/127	4223/112/78
RMS deviations (bond (Å)/angle (deg)/Plane (Å))[e]	0.011/1.503/0.095	0.012/1.651/0.089
average B factor (Å^2)	36.0	44.0
Ramachandran (favored/allowed (%))[f]	97.8/100.0	97.4/100.0
PDB ID	4XF7	4XF6

[a]Values for the outermost resolution shell are given in parentheses. [b]$R_{sym} = \sum|I_i - \langle I_i\rangle|/\sum\langle I_i\rangle$, where I_i is the observed intensity, and $\langle I_i\rangle$ is the average intensity over symmetry equivalent measurements. [c]$R = \sum||F_{obs}| - |F_{calc}||/\sum|F_{obs}|$. R_{free} is the same as R but for the 5% of reflection data excluded from refinement. [d]Solvent includes iodine anions. [e]Root-mean-square (RMS) deviations from ideal values. [f]Ramachandran analysis performed using Molprobity.[43,44]

the $F_o - F_c$ map calculated using the final refined model, suggesting that the mixed ligand assignment is reasonable. The statistics for the refined structures are summarized in Table 1.

Kinase Activity Measurement. The kinase activity of TK2285 was spectrophotometrically measured as described in a previous report.[4] The amount of the ADP produced by the TK2285 protein was determined by using two coupling enzymes, pyruvate kinase and lactate dehydrogenase. The produced ADP was coupled with pyruvate generation by pyruvate kinase and NADH consumption by lactate dehydrogenase. The reduction of NADH was detected by the absorbance at 340 nm (A_{340}) using a V-630 spectrophotometer (JASCO Corporation, Tokyo). The two enzymes, pyruvate kinase and lactate dehydrogenase, and ATP were purchased from Sigma-Aldrich (St. Louis, MO). NADH, phospho(enol)-pyruvate, and *myo*-inositol were purchased from Nacalai Tesque. In addition, (−)-*vibo*-quercitol (Hokko Chemical Industry Co. Ltd., Tokyo) was used as an alternative phosphate acceptor instead of *myo*-inositol.

The kinase activity measurement consisted of two steps. The reaction mixture for the first step (100 μL) was composed of 50 mM MES-NaOH (pH 6.5), 20 mM $MgCl_2$, 0.1−10 μg of TK2285 (the wild-type or the mutants), 0.1−300 mM *myo*-inositol, and 3 mM ATP. The effect of Na^+ or K^+ absence/presence for the activity has not been investigated in the present study since such monovalent cations are considered not to affect the TK2285 activity based on the previous work.[4] After preincubation at 85 °C for 3 min, the addition of ATP initiated the first reaction. The reactions were carried out at 85 °C for various durations and terminated by cooling on ice for 10 min. The TK2285 protein in the reaction mixture was removed with an Amicon Ultra centrifugal filter unit (MWCO 10,000), and the filtrate was used for the second step. The reaction mixture for the second step (100 μL) was composed of 50 mM MES-NaOH (pH 6.5), 0.2 mM NADH, 5 mM phospho(enol)-pyruvate, 1.8−3 units of pyruvate kinase, 2.7−4.2 units of lactate dehydrogenase, and 5−20 μL of the first reaction mixture. The second step of reactions were carried out at room temperature for 3 min, and their A_{340} values were measured. The decrease in A_{340} in a control experiment without *myo*-inositol was subtracted from the result of each assay.

Several assays were performed using different durations for the first reaction (e.g., 3, 4, 5, 6, 7, and 8 min), and the amounts of the ADP produced from the kinase reaction of TK2285 were calculated. Initial velocities of the *myo*-inositol kinase reaction were determined as the slope in the plot of the reaction time against the amounts of the produced ADP. The values of k_{cat} and K_m for the wild-type and Q136A and R140A mutants were analyzed by a nonlinear regression using the Michaelis−Menten equation with the program SigmaPlot.

Analysis of the TK2285 Product. The NMR sample was prepared as described below. The reaction product mixture (200 μL) contained 100 mM ammonium acetate (pH 6.65), 10 mM $MgCl_2$, 8 mM ATP, 6 mM *myo*-inositol, and 5 μg of TK2285 in the reaction buffer. After preincubation at 85 °C for 3 min, the reaction was initiated by adding ATP, continued at 85 °C for 5 min, and terminated by rapid cooling on ice for 10 min. The enzyme in the reaction mixture was removed with an Amicon Ultra centrifugal filter unit (MWCO 10,000), and the filtrate was used as the reaction product mixture. The NMR sample was prepared by diluting 140 μL of the reaction product mixture with 360 μL of the D_2O solution for field-lock.

All of the NMR measurements were carried out on an ECS-400 spectrometer (JEOL, Tokyo) at 400 MHz and 30 °C. The chemical shifts of the ^1H and ^{31}P NMR spectra were given in ppm relative to the signals of solvents using external standards of D_2O at 4.62 ppm and 85% H_3PO_4 at 0.00 ppm, respectively. The 1D-^1H NMR and 2D-^1H−^1H COSY spectra were acquired using a pulse sequence incorporating presaturation for water suppression. The presaturation power was 56 dB, which is the

DOI: 10.1021/acs.biochem.5b00296
Biochemistry 2015, 54, 3494−3503

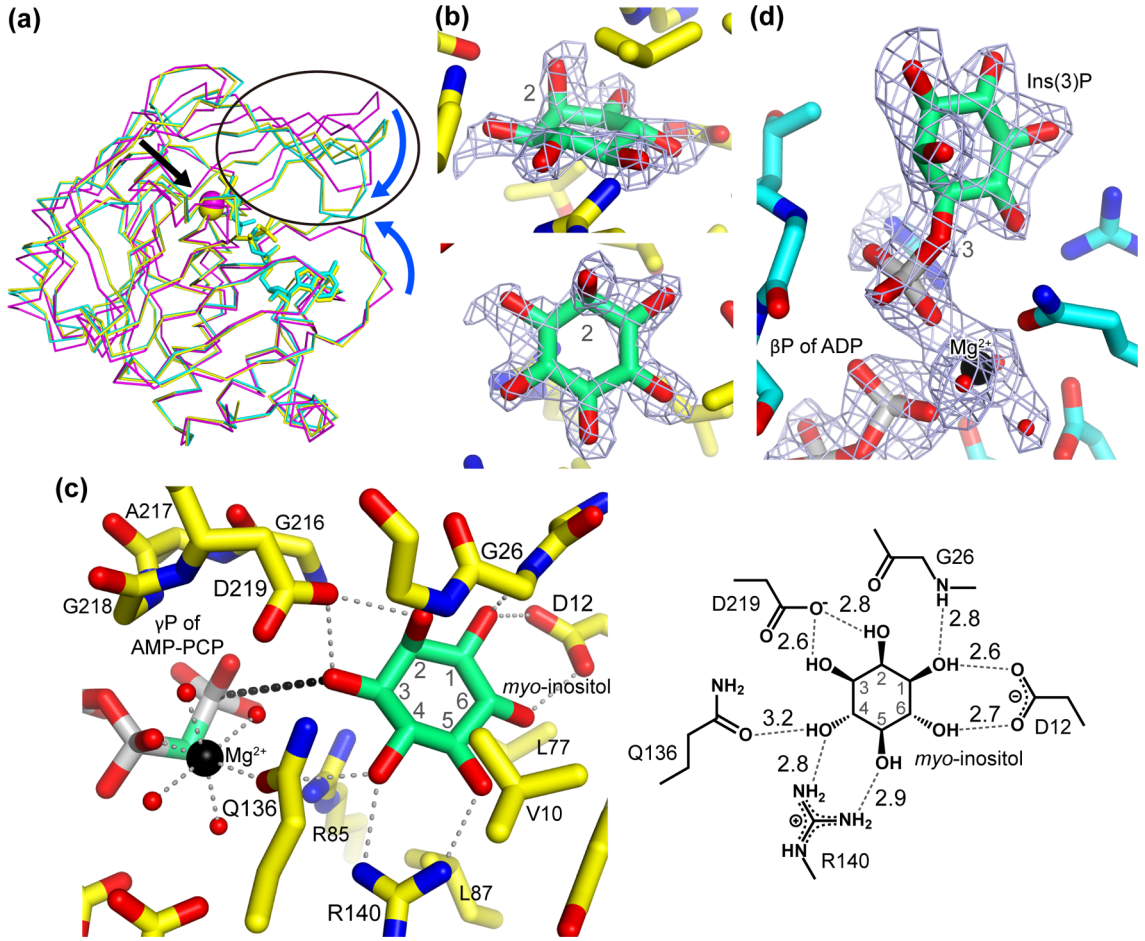

Figure 1. Structures of TK2285. The gray characters around the *myo*-inositol carbons represent the atom numbering. (a) Superposition of the ternary substrates-complex (yellow) and the ternary products-complex (cyan) on the unliganded (magenta) structure. The ellipse shows the lid domain. The blue arrows display the conformational changes around the active site induced by ligand-binding. The black arrow indicates the Cα atoms of G26 of TK2285 shown as spheres. (b) $F_o - F_c$ omit electron density map for the *myo*-inositol contoured at 3 σ superposed on the refined structure of the ternary substrates-complex. The two panels are drawn from the two different viewpoints. TK2285 residues and the *myo*-inositol molecule are shown using yellow and green sticks, respectively. (c) Active site of the ternary substrates-complex. Residues of TK2285, *myo*-inositol, and AMP-PCP are shown with stick models. Mg^{2+} and water molecules are shown as black and red spheres, respectively. Gray broken lines show interactions with *myo*-inositol and Mg^{2+}. A black broken line is drawn between the γ-phosphate of AMP-PCP and the 3-hydroxyl group of *myo*-inositol. The schematic diagram (right panel) shows the distances between *myo*-inositol and the residues in Å. (d) $F_o - F_c$ omit electron density map of the ternary products-complex contoured at 3σ superposed on the refined structure of the complex. Ins(3)P, ADP, Mg^{2+}, and the waters around Mg^{2+} were omitted from the map calculation.

minimum required for complete suppression of the water peak. The 1D-^{1}H−^{1}H TOCSY was acquired without the water presaturation pulse sequence. Selective TOCSY measurements of *myo*-inositol monophosphate with the excitation at the proton of H-2 (at 4.20 ppm) or H-5 (at 3.27 ppm) were performed using a selected power of 58.7 dB and mixing time of 50 ms. In order to identify the ^{1}H−^{31}P linkages, the 1-bond ($^1J_{HP}$) and the long-range ($^nJ_{HP}$) linkage couplings were set to 200 and 10 Hz, respectively.

The LC-MS sample was prepared in the same manner as that described above for the NMR sample, with the exception that 10 mM ATP was used. After filtration to remove the enzyme, the sample was analyzed by LC-MS using an Accela 600 HPLC system and an EXACTIVE mass spectrometer (Thermo Fisher Scientific, San Jose, CA) equipped with an electrospray ionization source. A CHIRALPAK QN-AX chiral column (Daicel Corporation, Tokyo) and a buffer composed of 94.1:4.7:0.9:0.3 volumes of methanol, water, acetic acid, and triethylamine were utilized as the column and mobile phase for LC, respectively. After the column development at a flow rate of 1 mL min^{-1} for 25 min, the sample was separated by LC. Eluted *myo*-inositol monophosphate was detected by mass spectrometry with a mass range of m/z 259.0211−259.0237. The electrospray ionization source was operated in the negative ion mode. Authentic 1-D-*myo*-inositol 1-phosphate (Ins(1)P) and Ins(3)P were purchased from Cayman Chemical Company (Ann Arbor, MI).

RESULTS

Crystal Structure of the Ternary Substrates-Complex of TK2285. The purified sample for crystallization showed apparent homogeneity in Native- and SDS−PAGE (data not shown). The crystals of the ternary substrates-complex were obtained by the cocrystallization of *myo*-inositol, AMP-PCP, and the enzyme. AMP-PCP, which is a nonhydrolyzable ATP analogue and thus does not allow phosphate transfer, was used to elucidate the ternary substrates-complex structure just before the kinase reaction. The ternary substrates-complex structure

DOI: 10.1021/acs.biochem.5b00296
Biochemistry 2015, 54, 3494−3503

was determined at 1.93 Å resolution with the crystallographic R and R_{free} factors of 21.6% and 25.5%, respectively (Table 1). An asymmetric unit of the crystal is composed of two TK2285 molecules, and the structures of the two molecules are very similar to each other. Superposition of the ternary substrates-complex on the unliganded structure[4] (root-mean-square (RMS) distances 1.0 Å for all 273 Cα atoms) showed that the active site is closed especially by the lid domain transformation of the ternary substrates-complex (Figure 1a). The corresponding conformational change has been reported in ribokinase and is thought to increase the affinity toward ATP.[14] The movement in TK2285 is considered to be induced by the interaction between *myo*-inositol and the glycine-rich motif, especially with the residue G26, as shown in ribokinase (Figure 1a).[14]

The crystal structure of the ternary substrates-complex provides several insights into the substrate-binding mechanism of TK2285. This structure possesses AMP-PCP, *myo*-inositol, and Mg^{2+} in the active site of TK2285. The $F_o - F_c$ omit electron density map shows that the structure of *myo*-inositol in the active site is in a chair conformation in which the 2-hydroxyl group is axial (Figure 1b). All six of the hydroxyl groups of *myo*-inositol interact with five residues (D12, G26, Q136, R140, and D219) of TK2285 (Figure 1c), which is consistent with the 100−1000-fold stronger affinity toward *myo*-inositol compared to that of various sugars.[4] The side chain amido group of Q136 is located close to Mg^{2+} and the 4-hydroxyl group of the ligand (2.16 and 3.24 Å, respectively). This led us to hypothesize that Q136 contributes not only to *myo*-inositol binding but also to Mg^{2+} binding. The six-membered carbon ring of *myo*-inositol interacts with three hydrophobic residues (V10, L77, and L87). The recognition of AMP-PCP by TK2285 resembles those of other ribokinase family members.[3] The γ-phosphate of AMP-PCP is surrounded by the main-chain nitrogen atoms of G216−D219 and the side chain of R85. The Mg^{2+} is octahedrally coordinated by the β-phosphate of AMP-PCP, Q136, and four water molecules. The 3-hydroxyl group of *myo*-inositol is nearest to the γ-phosphate of AMP-PCP and interacts with D219, which is thought to deprotonate the hydroxyl group of the phosphate acceptor (Figure 1c). This result suggests that the 3-hydroxyl group is phosphorylated by the TK2285 kinase reaction.

Roles of the *myo*-Inositol-Binding Residues. Kinase activity measurements of TK2285 mutant proteins were performed in order to examine the roles of the residues interacting with *myo*-inositol in the crystal structure as described above. The amino acid sequence alignment showed that the five interacting residues are conserved in the *myo*-inositol kinase (Lpa3) from *Zea mays* (Table 2). Q136 is the most interesting residue to investigate since this residue interacts with Mg^{2+} in addition to *myo*-inositol. Two of the other four residues (D12 and R140) were also investigated to estimate their contribution to *myo*-inositol binding. In the case of the other two residues (G26 and D219), although they interact with the *myo*-inositol molecule, they were not investigated for the following reasons. Replacement of G26 into any residue is considered to prevent a *myo*-inositol molecule from binding due to steric hindrance. D219 is known to be the essential residue for catalysis conserved in ribokinase family proteins, and mutation of this aspartate residue is predicted to result in impairment of the kinase activity. Thus, the kinase activities of the three mutants (D12A, Q136A, and R140A) and the wild-type of TK2285 were measured.

Table 2. Conservation of the Five Residues Interacting with *myo*-Inositol in the Ribokinase Family[a]

TK2285	D12	G26	Q136	R140	D219
Lpa3	D	G	Q	R	D
NK	D	G	G	P	D
AK	D	G	S	A, F, V	D
RK	D	G	A		D
KDGK	A, Q, R	G	N	R	D
T6PK	D	G		A	D
FK	D	G	E		D
AIRK	D	G	N	S	D
PFK2	D	G	S		D
PK	H, S	A, V	V	D, V, Y	C, D
HMPPK	S	A	V	L	C
AGK	D	G	A	A, T	D
APFK	D	G	A	Q	D
THZK			V	G	C

[a]Except for Lpa3, residues corresponding to the five residues interacting with *myo*-inositol in TK2285 were selected based on the three-dimensional structure superposition (Figure S3, Supporting Information). For Lpa3, corresponding residues found by the primary sequence alignment using ClustalW are represented. Abbreviations; NK, nucleoside kinase; AK, adenosine kinase; RK, ribokinase; KDGK, 2-keto-3-deoxygluconate kinase; T6PK, tagatose-6-phosphate kinase; FK, fructokinase; AIRK, aminoimidazole riboside kinase; PFK2, phosphofructokinase-2; PK, pyridoxal kinase; HMPPK, 4-amino-5-hydroxymethyl-2-methylpyrimidine phosphate kinase; AGK, ADP-dependent glucokinase; APFK, ADP-dependent phosphofructokinase; THZK, 4-methyl-5-β-hydroxyethyl thiazole kinase.

The results of the enzymatic assays are shown in Figure 2 and Table 3. The reactions of the wild-type, Q136A, and

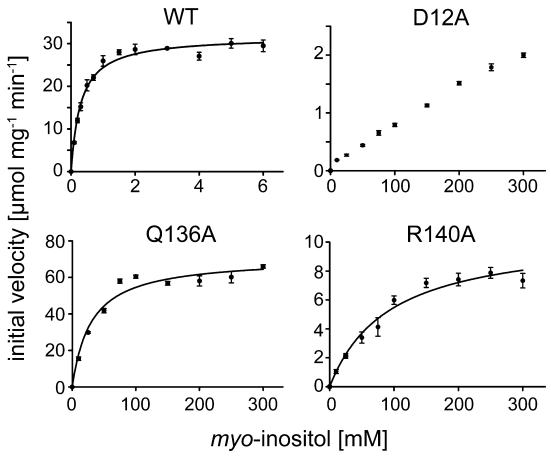

Figure 2. Kinase activity of the wild-type (WT) and the three mutants (D12A, Q136A, and R140A). The vertical and the horizontal axes represent the initial velocity and the concentrations of *myo*-inositol, respectively.

Table 3. Kinetics Parameters of the Reaction toward *myo*-Inositol

	WT	D12A	Q136A	R140A
k_{cat} [s^{-1}]	15.9 ± 0.3	n.d.[a]	36 ± 2	5.3 ± 0.4
K_m [mM]	0.30 ± 0.03	n.d.[a]	30 ± 6	92 ± 19

[a]n.d.: not determined due to a drastic decrease in affinity toward *myo*-inositol.

DOI: 10.1021/acs.biochem.5b00296
Biochemistry 2015, 54, 3494−3503

R140A with varying concentrations of *myo*-inositol followed Michaelis–Menten kinetics. In contrast, the initial velocity of the D12A reaction is almost proportional to the substrate concentration (Figure 2), most likely due to a drastic decrease in affinity toward *myo*-inositol (increase in K_m). Thus, the k_{cat} and K_m values of this mutant could not be determined. The detection of kinase activity in the Q136A mutant and the requirement of Mg^{2+} for the TK2285 reaction[4] suggest that the interaction between Q136 and the Mg^{2+} contributes to but is not essential for Mg^{2+} binding to the TK2285 protein and catalysis. The K_m values of the Q136A and R140A mutants toward *myo*-inositol are at least 100-fold higher than that of the wild-type (Table 3). These results suggest that these three residues are important for *myo*-inositol binding.

Crystal Structure of the Ternary Products-Complex of TK2285. The crystals of the ternary products-complex were obtained by using a mixture of the TK2285 protein and the substrates, *myo*-inositol and ATP. The mixture was incubated at 85 °C for 5 min in order to allow the enzyme to convert the substrates into the products. Using the crystals, the ternary products-complex structure was determined at 2.08 Å resolution with the crystallographic R and R_{free} factors of 20.3% and 25.0%, respectively (Table 1). An asymmetric unit of the crystal is composed of two TK2285 molecules, and the two molecules are very similar to each other in structure. Structural superposition showed that the lid domain of the ternary products-complex is transformed from the unliganded structure[4] and covers the substrate pocket (RMS distances 1.1 Å for all 273 Cα atoms). The overall structure of the ternary products-complex is very similar to that of the ternary substrates-complex (RMS distances 0.4 Å for all 273 Cα atoms; Figure 1a).

In the active site of the ternary products-complex, ADP and Ins(3)P molecules as well as Mg^{2+} were found (Figure 1d). Electron density maps corresponding to the β-phosphate of ADP and the phosphate group of Ins(3)P are clearly distinguished and bridged by the Mg^{2+}. This structure clearly shows that ADP and Ins(3)P are produced in the TK2285 kinase reaction (Figure 3).

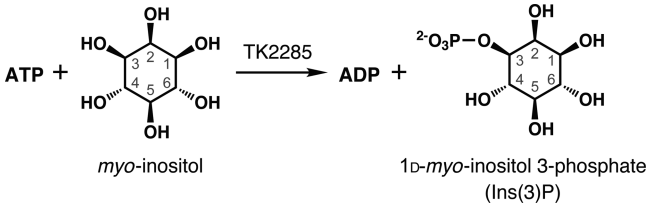

Figure 3. Kinase reaction catalyzed by TK2285. The atom numbering of *myo*-inositol carbons is shown by the gray numbers.

Analysis of the TK2285 Product. In order to confirm the phosphorylated hydroxyl group of the TK2285 product, we took the NMR spectra for the reaction mixtures with and without the TK2285 protein. The spectrum for the reaction product mixture showed two characteristic peaks (4.18 and 3.26 ppm, arrows in Figure 4c), which were not seen in the spectrum for the reaction mixture without the enzyme (Figure 4b). 1D-TOCSY analyses using radiofrequency irradiation at these two peaks revealed that the peaks at 4.18, 3.87, 3.68, 3.57, 3.49, and 3.26 ppm correspond to the product *myo*-inositol monophosphate (triangles in Figures 4d and e). The cross-peaks of $^1H-^1H$ COSY analysis (Figure 5a) and the reference

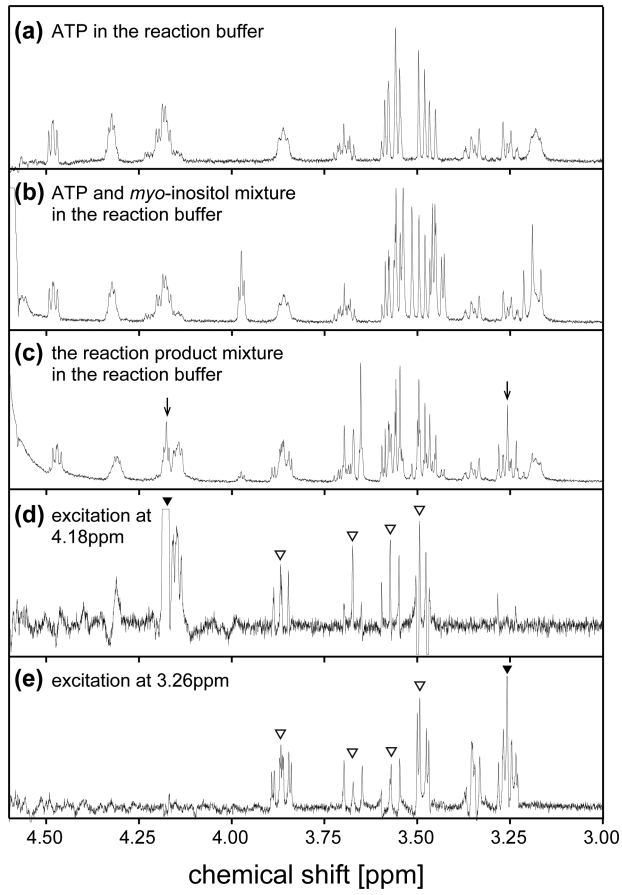

Figure 4. 1D NMR spectra. ^1H NMR spectra for (a) ATP in the reaction buffer, (b) ATP and *myo*-inositol mixture in the reaction buffer, and (c) the reaction product mixture prepared by the incubation of ATP and *myo*-inositol with the enzyme in the reaction buffer. Arrows indicate two characteristic peaks for the product. (d and e) $^1H-^1H$ TOCSY spectra (excited at 4.18 or 3.26 ppm, respectively) for the reaction product mixture, which is the same solution as that of panel c. Closed and open triangles represent the selective excitations and the emphasized peaks for the product, respectively.

values[15] identified that these six peaks correspond to 2-H, 1/3-H, 4/6-H, 4/6-H, 1/3-H, and 5-H. Because of the mirror symmetry of the *myo*-inositol molecule, it is impossible to distinguish 1-H and 3-H as well as 4-H and 6-H by NMR. $^1H-^{31}P$ HMBC analysis with irradiation at the phosphate site of the *myo*-inositol phosphate (2.65 ppm) revealed that the phosphate group of *myo*-inositol is strongly related to the 1/3-H (3.87 ppm) and weakly related to 2-H (4.18 ppm) and 4/6H (3.68 ppm) (Figure 5b). This analysis indicates that either the 3-OH or the 1-OH group of *myo*-inositol is phosphorylated. All spectra, including those of the control experiments and their interpretations are shown in the Supporting Information (Figures S1 and S2).

Finally, we analyzed the TK2285 reaction product with HPLC using a chiral column and a mass spectrometry system to distinguish whether the reaction product was either (Ins(1)P) or Ins(3)P. The analysis using a CHIRALPAK QN-AX chiral column showed that the retention time of the TK2285 product was consistent with that of Ins(3)P but not with that of Ins(1)P (Figure 6). These analyses demonstrated that the TK2285 reaction product is Ins3(P). This is supported by the fact that no significant TK2285 kinase activity toward (−)-*vibo*-quercitol, which is a 1D-*myo*-inositol derivative lacking

DOI: 10.1021/acs.biochem.5b00296
Biochemistry 2015, 54, 3494–3503

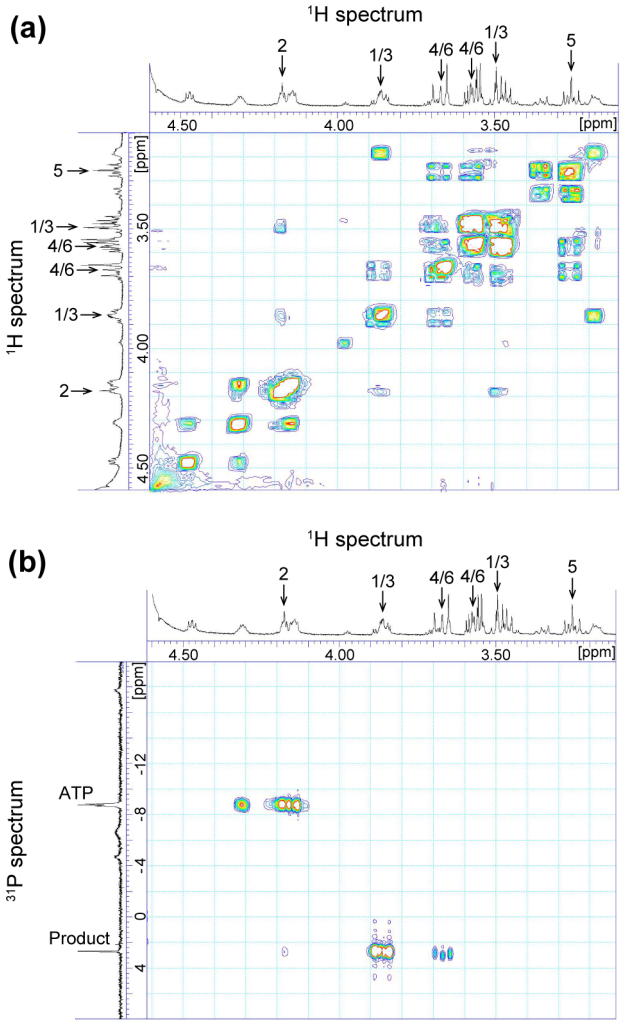

Figure 5. 2D NMR spectra. (a) $^{1}H-^{1}H$ COSY and (b) $^{1}H-^{31}P$ HMBC for the reaction product mixture. Arrows indicate the peaks corresponding to the protons of the product.

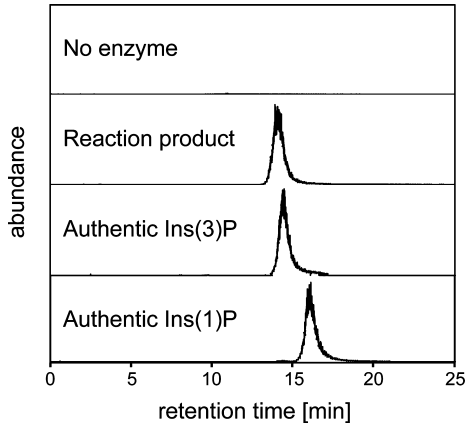

Figure 6. LC-MS analyses using a chiral column. Eluted *myo*-inositol monophosphate was detected by mass spectrometry with a mass range of m/z 259.0211−259.0237. No enzyme: ATP and *myo*-inositol mixture in the reaction buffer. Reaction product: the reaction product mixture. Authentic Ins(3)P and authentic Ins(1)P: authentic compounds. The reaction product and authentic Ins(3)P eluted at the same retention time.

the 3-OH, was detected (data not shown). Thus, we propose that TK2285 is designated *myo*-inositol 3-kinase (MI3K).

DISCUSSION

Identification of the phosphorylated derivatives of *myo*-inositol is important for understanding *myo*-inositol metabolism, but the mirror symmetry of the *myo*-inositol molecule structure makes such identification difficult. Two methods have been reported for distinguishing the enantiomeric derivatives. The first one utilizes optical rotation. However, the specific rotations for some inositol derivatives are subtle and highly sensitive to pH. For example, the $[\alpha]_D$ values of Ins(1)P at pH 9 and pH 2 are +4.4 and −6.1, respectively; they are very small, and their signs (plus or minus) are different from each other.[15] In addition, intensive purification is required to measure the optical value since various biomolecules that consist of chiral centers in their molecular structure interfere with the optical value measurement. These drawbacks make it difficult to rely on optical rotation. The second method utilizes chiral columns. Both HPLC and gas chromatography analyses have been used for the enantiomeric analysis of *myo*-inositol derivatives. The reported gas chromatography analysis requires derivatization of Ins(3)P by trimethylsilylation followed by the methylation of phosphate.[16] The reported HPLC analysis was performed to distinguish the enantiomers of the benzylated precursor of *myo*-inositol phosphate.[17] No method has been reported for directly identifying the enantiomers of *myo*-inositol monophosphates without purification and/or derivation steps. Our method using HPLC with a CHIRALPAK QN-AX chiral column enables much easier identification of the enantiomers of inositol phosphate.

Dali server analysis[18] disclosed 28 enzymes whose structures resembled the structure of MI3K. All of these enzymes belong to the ribokinase family and in total catalyze 13 distinct kinase reactions. Table 2 summarizes the conservation of the five residues (represented in Figure S3, Supporting Information) interacting with *myo*-inositol in the 13 kinds of enzymes based on the three-dimensional structure superpositions. G26 is conserved in almost all of the enzymes except for pyridoxal kinase (PK), 4-amino-5-hydroxymethyl-2-methylpyrimidine phosphate kinase (HMPPK) and 4-methyl-5-β-hydroxyethyl thiazole kinase (THZK). PK[19−24] and HMPPK[25] utilize valine or alanine residues to recognize the aromatic ring of the substrate. D219 is also conserved in almost all of the enzymes except for PK from *Bacillus subtilis*,[23] HMPPK, and THZK.[26] The corresponding aspartate residues of these enzymes are thought to deprotonate the hydroxyl group of the phosphate acceptors.[3] D12 is conserved in the enzymes except for 2-keto-3-deoxygluconate kinases (KDGK), PK, HMPPK, and THZK. In almost all of the other enzymes, the residues corresponding to D12 interact with the furanose (pyranose) ring of the phosphate acceptors.[16,27−38] However, Q136 is not conserved in any of the 13 kinds of enzymes, and R140 is conserved only in KDGK in addition to *myo*-inositol kinase. These two residues are conserved in Lpa3, the *myo*-inositol kinase from *Zea mays* (Table 2). Thus, possessing both of the two residues may be a characteristic of *myo*-inositol kinases.

Our investigations revealed that MI3K (encoded by TK2285) phosphorylates the 3-hydroxyl group of *myo*-inositol. The synthesized Ins(3)P is thought to be incorporated into the metabolism of *T. kodakarensis*. The first step of the *myo*-inositol metabolism in *T. kodakarensis* is considered to be the conversion of glucose 6-phosphate to Ins(3)P by Ins(3)P

DOI: 10.1021/acs.biochem.5b00296
Biochemistry 2015, 54, 3494−3503

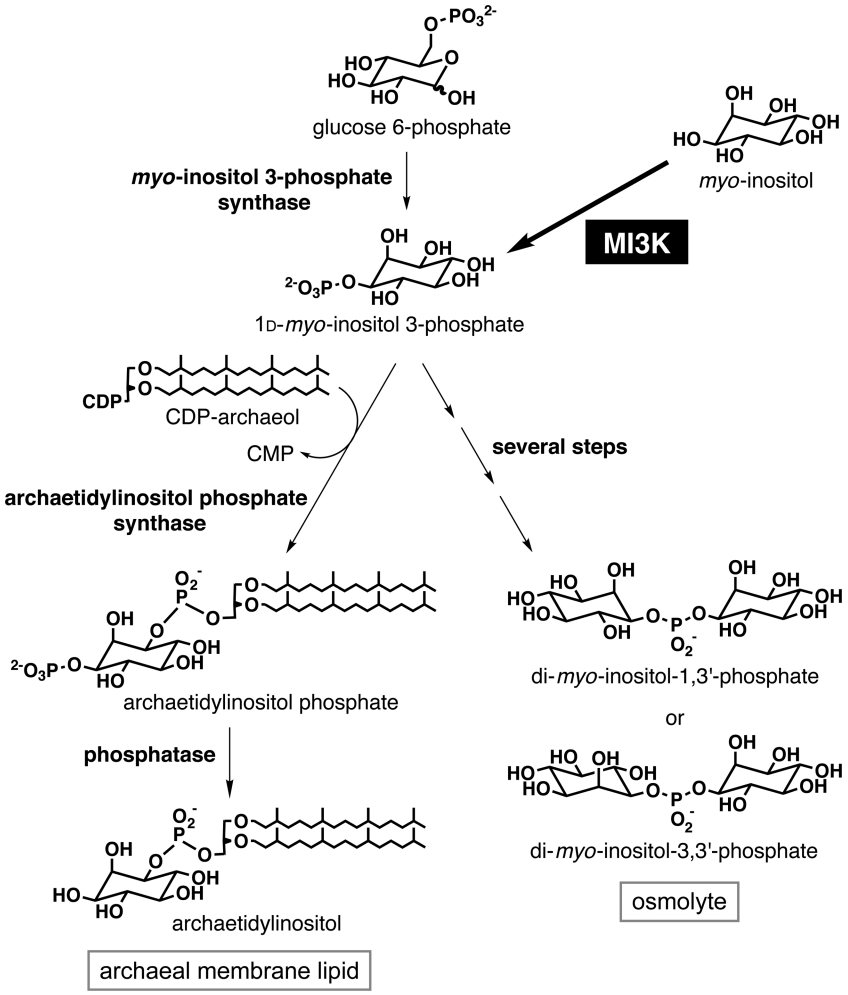

Figure 7. Predicted *myo*-inositol metabolism in *T. kodakarensis*.

synthase.[16,39−41] This Ins(3)P can be a precursor for archaeal membrane lipids or osmolytes (Figure 7). MI3K may also supply Ins(3)P to this metabolic pathway. Di-*myo*-inositol phosphate is known to exist in *T. kodakarensis* cells as an osmolyte at concentrations of 4 mM in the absence of heat shock stress,[42] while the concentration increases up to 80 mM under heat shock conditions.[42] The excess di-*myo*-inositol phosphate is possibly degraded to *myo*-inositol under nonstress conditions.[4] MI3K may contribute in salvaging the degraded *myo*-inositol molecules. Further investigations of *myo*-inositol metabolism may lead to the elucidation of a new metabolic pathway in *T. kodakarensis*.

■ ASSOCIATED CONTENT

Supporting Information

Detailed explanation of the NMR analyses; 2D NMR spectra; 1D NMR spectra; and structural sequence alignment of the ribokinase family. The Supporting Information is available free of charge on the ACS Publications website at DOI: 10.1021/acs.biochem.5b00296.

■ AUTHOR INFORMATION

Corresponding Author

*Tel.: 81-75-753-4029. Fax: 81-75-753-4032. E-mail: miki@kuchem.kyoto-u.ac.jp.

Funding

This work was partially supported by a Grant-in-Aid for Young Scientists (B) to T.S. (JSPS KAKENHI Grant Number 26850049).

Notes

The authors declare no competing financial interest.

■ ACKNOWLEDGMENTS

We are grateful to Dr. Takuya Hashimoto for the helpful discussions, to the staff members at the beamlines of the Photon Factory for their help with the data collection, and to DAICEL Corporation CPI company for their support in identifying the chiral compounds by HPLC. We would also like to express our gratitude to Ms. Karin Nishimura for MS analyses and Ms. Eriko Kusaka for NMR analyses. Use of the beamlines at the Photon Factory was approved by the Photon Factory Advisory Committee (Proposal 2014G189).

■ ABBREVIATIONS

AMP-PCP, β,γ-methyleneadenosine 5′-triphosphate; DTT, dithiothreitol; HMPPK, 4-amino-5-hydroxymethyl-2-methylpyrimidine phosphate kinase; Ins(1)P, 1D-*myo*-inositol 1-phosphate; Ins(3)P, 1D-*myo*-inositol 3-phosphate; KDGK, 2-keto-3-deoxygluconate kinases; MI3K, *myo*-inositol 3-kinase; PAGE, polyacrylamide gel electrophoresis; PCR, polymerase

DOI: 10.1021/acs.biochem.5b00296
Biochemistry 2015, 54, 3494−3503

chain reaction; PDB, Protein Data Bank; PK, pyridoxal kinase; THZK, 4-methyl-5-β-hydroxyethyl thiazole kinase

REFERENCES

(1) Verhees, C. H., Kengen, S. W., Tuininga, J. E., Schut, G. J., Adams, M. W., De Vos, W. M., and Van Der Oost, J. (2003) The unique features of glycolytic pathways in Archaea. *Biochem. J. 375*, 231−246.

(2) Bork, P., Sander, C., and Valencia, A. (1993) Convergent evolution of similar enzymatic function on different protein folds: the hexokinase, ribokinase, and galactokinase families of sugar kinases. *Protein Sci. 2*, 31−40.

(3) Park, J., and Gupta, R. S. (2008) Adenosine kinase and ribokinase-the RK family of proteins. *Cell. Mol. Life Sci. 65*, 2875−2896.

(4) Sato, T., Fujihashi, M., Miyamoto, Y., Kuwata, K., Kusaka, E., Fujita, H., Miki, K., and Atomi, H. (2013) An uncharacterized member of the ribokinase family in *Thermococcus kodakarensis* exhibits *myo*-inositol kinase activity. *J. Biol. Chem. 288*, 20856−20867.

(5) Shi, J., Wang, H., Hazebroek, J., Ertl, D. S., and Harp, T. (2005) The maize *low-phytic acid 3* encodes a *myo*-inositol kinase that plays a role in phytic acid biosynthesis in developing seeds. *Plant J. 42*, 708−719.

(6) International Union of Pure and Applied Chemistry (IUPAC) and International Union of Biochemistry (IUB). (1968) Tentative rules for cyclitol nomenclature. *J. Biol. Chem. 243*, 5809−5819.

(7) Nomenclature Committee of the International Union of Biochemistry (NC-IUB). (1989) Numbering of atoms in *myo*-inositol. Recommendations 1988. *Eur. J. Biochem. 180*, 485−486.

(8) Irvine, R. F., and Schell, M. J. (2001) Back in the water: the return of the inositol phosphates. *Nat. Rev. Mol. Cell Biol. 2*, 327−338.

(9) Gasteiger, E., Hoogland, C., Gattiker, A., Duvaud, S., Wilkins, M. R., Appel, R. D., and Bairoch, A. (2005) Protein Identification and Analysis Tool on the ExPASy Server, in *The Proteomics Protocols Handbook* (Walker, J. M., Ed.) pp 571−607, Humana Press, Totowa, NJ.

(10) Otwinowski, Z., and Minor, W. (1997) Processing of X-ray Diffraction Data Collected in Oscillation Mode, in *Methods in Enzymology* (Carter, C. W., Jr., and Sweet, R. M., Eds.) pp 307−326, Academic Press, New York.

(11) Emsley, P., Lohkamp, B., Scott, W. G., and Cowtan, K. (2010) Features and development of Coot. *Acta Crystallogr., Sect. D 66*, 486−501.

(12) Collaborative Computational Project, Number 4 (1994) The CCP4 suite: programs for protein crystallography. *Acta Crystallogr., Sect. D 50*, 760−763.

(13) Murshudov, G. N., Vagin, A. A., Lebedev, A., Wilson, K. S., and Dodson, E. J. (1999) Efficient anisotropic refinement of macromolecular structures using FFT. *Acta Crystallogr., Sect. D 55*, 247−255.

(14) Sigrell, J. A., Cameron, A. D., and Mowbray, S. L. (1999) Induced fit on sugar binding activates ribokinase. *J. Mol. Biol. 290*, 1009−1018.

(15) Podeschwa, A. L. M., Plettenburg, O., and Altenbach, H.-J. (2005) Flexible stereo- and regioselective synthesis of *myo*-inositol phosphates (part 1): Via symmetrical conduritol B derivatives. *Eur. J. Org. Chem. 2005*, 3101−3115.

(16) Morii, H., Kiyonari, S., Ishino, Y., and Koga, Y. (2009) A novel biosynthetic pathway of archaetidyl-*myo*-inositol via archaetidyl-*myo*-inositol phosphate from CDP-archaeol and D-glucose 6-phosphate in methanoarchaeon *Methanothermobacter thermautotrophicus* cells. *J. Biol. Chem. 284*, 30766−30774.

(17) Sculimbrene, B. R., Morgan, A. J., and Miller, S. J. (2002) Enantiodivergence in small-molecule catalysis of asymmetric phosphorylation: concise total syntheses of the enantiomeric D-*myo*-inositol-1-phosphate and D-*myo*-inositol-3-phosphate. *J. Am. Chem. Soc. 124*, 11653−11656.

(18) Holm, L., and Rosenström, P. (2010) Dali server: conservation mapping in 3D. *Nucleic Acids Res. 38*, W545−549.

(19) Jones, D. C., Alphey, M. S., Wyllie, S., and Fairlamb, A. H. (2012) Chemical, genetic and structural assessment of pyridoxal kinase as a drug target in the African trypanosome. *Mol. Microbiol. 86*, 51−64.

(20) Li, M. H., Kwok, F., Chang, W. R., Liu, S. Q., Lo, S. C., Zhang, J. P., Jiang, T., and Liang, D. C. (2004) Conformational changes in the reaction of pyridoxal kinase. *J. Biol. Chem. 279*, 17459−17465.

(21) Badger, J., Sauder, J. M., Adams, J. M., Antonysamy, S., Bain, K., Bergseid, M. G., Buchanan, S. G., Buchanan, M. D., Batiyenko, Y., Christopher, J. A., Emtage, S., Eroshkina, A., Feil, I., Furlong, E. B., Gajiwala, K. S., Gao, X., He, D., Hendle, J., Huber, A., Hoda, K., Kearins, P., Kissinger, C., Laubert, B., Lewis, H. A., Lin, J., Loomis, K., Lorimer, D., Louie, G., Maletic, M., Marsh, C. D., Miller, I., Molinari, J., Muller-Dieckmann, H. J., Newman, J. M., Noland, B. W., Pagarigan, B., Park, F., Peat, T. S., Post, K. W., Radojicic, S., Ramos, A., Romero, R., Rutter, M. E., Sanderson, W. E., Schwinn, K. D., Tresser, J., Winhoven, J., Wright, T. A., Wu, L., Xu, J., and Harris, T. J. (2005) Structural analysis of a set of proteins resulting from a bacterial genomics project. *Proteins 60*, 787−796.

(22) Gandhi, A. K., Ghatge, M. S., Musayev, F. N., Sease, A., Aboagye, S. O., di Salvo, M. L., Schirch, V., and Safo, M. K. (2009) Kinetic and structural studies of the role of the active site residue Asp235 of human pyridoxal kinase. *Biochem. Biophys. Res. Commun. 381*, 12−15.

(23) Newman, J. A., Das, S. K., Sedelnikova, S. E., and Rice, D. W. (2006) The crystal structure of an ADP complex of *Bacillus subtilis* pyridoxal kinase provides evidence for the parallel emergence of enzyme activity during evolution. *J. Mol. Biol. 363*, 520−530.

(24) Safo, M. K., Musayev, F. N., di Salvo, M. L., Hunt, S., Claude, J. B., and Schirch, V. (2006) Crystal structure of pyridoxal kinase from the *Escherichia coli* pdxK gene: implications for the classification of pyridoxal kinases. *J. Bacteriol. 188*, 4542−4552.

(25) Cheng, G., Bennett, E. M., Begley, T. P., and Ealick, S. E. (2002) Crystal structure of 4-amino-5-hydroxymethyl-2-methylpyrimidine phosphate kinase from *Salmonella typhimurium* at 2.3 Å resolution. *Structure 10*, 225−235.

(26) Campobasso, N., Mathews, I. I., Begley, T. P., and Ealick, S. E. (2000) Crystal structure of 4-methyl-5-beta-hydroxyethylthiazole kinase from *Bacillus subtilis* at 1.5 Å resolution. *Biochemistry 39*, 7868−7877.

(27) Arnfors, L., Hansen, T., Schönheit, P., Ladenstein, R., and Meining, W. (2006) Structure of *Methanocaldococcus jannaschii* nucleoside kinase: an archaeal member of the ribokinase family. *Acta Crystallogr., Sect. D 62*, 1085−1097.

(28) Yasutake, Y., Ota, H., Hino, E., Sakasegawa, S., and Tamura, T. (2011) Structures of *Burkholderia thailandensis* nucleoside kinase: implications for the catalytic mechanism and nucleoside selectivity. *Acta Crystallogr., Sect. D 67*, 945−956.

(29) Reddy, M. C., Palaninathan, S. K., Shetty, N. D., Owen, J. L., Watson, M. D., and Sacchettini, J. C. (2007) High resolution crystal structures of *Mycobacterium tuberculosis* adenosine kinase: insights into the mechanism and specificity of this novel prokaryotic enzyme. *J. Biol. Chem. 282*, 27334−27342.

(30) Schumacher, M. A., Scott, D. M., Mathews, I. I., Ealick, S. E., Roos, D. S., Ullman, B., and Brennan, R. G. (2000) Crystal structures of *Toxoplasma gondii* adenosine kinase reveal a novel catalytic mechanism and prodrug binding. *J. Mol. Biol. 298*, 875−893.

(31) Cassera, M. B., Ho, M. C., Merino, E. F., Burgos, E. S., Rinaldo-Matthis, A., Almo, S. C., and Schramm, V. L. (2011) A high-affinity adenosine kinase from *Anopheles gambiae*. *Biochemistry 50*, 1885−1893.

(32) Kuettel, S., Greenwald, J., Kostrewa, D., Ahmed, S., Scapozza, L., and Perozzo, R. (2011) Crystal structures of *T. b. rhodesiense* adenosine kinase complexed with inhibitor and activator: implications for catalysis and hyperactivation. *PLoS Negl. Trop. Dis. 5*, e1164.

(33) Mathews, I. I., Erion, M. D., and Ealick, S. E. (1998) Structure of human adenosine kinase at 1.5 Å resolution. *Biochemistry 37*, 15607−15620.

DOI: 10.1021/acs.biochem.5b00296
Biochemistry 2015, 54, 3494−3503

(34) Trinh, C. H., Asipu, A., Bonthron, D. T., and Phillips, S. E. (2009) Structures of alternatively spliced isoforms of human ketohexokinase. *Acta Crystallogr., Sect. D 65*, 201−211.
(35) Zhang, Y., Dougherty, M., Downs, D. M., and Ealick, S. E. (2004) Crystal structure of an aminoimidazole riboside kinase from *Salmonella enterica*: implications for the evolution of the ribokinase superfamily. *Structure 12*, 1809−1821.
(36) Cabrera, R., Ambrosio, A. L., Garratt, R. C., Guixé, V., and Babul, J. (2008) Crystallographic structure of phosphofructokinase-2 from *Escherichia coli* in complex with two ATP molecules. Implications for substrate inhibition. *J. Mol. Biol. 383*, 588−602.
(37) Ito, S., Fushinobu, S., Jeong, J. J., Yoshioka, I., Koga, S., Shoun, H., and Wakagi, T. (2003) Crystal structure of an ADP-dependent glucokinase from *Pyrococcus furiosus*: implications for a sugar-induced conformational change in ADP-dependent kinase. *J. Mol. Biol. 331*, 871−883.
(38) Rivas-Pardo, J. A., Herrera-Morande, A., Castro-Fernandez, V., Fernandez, F. J., Vega, M. C., and Guixé, V. (2013) Crystal structure, SAXS and kinetic mechanism of hyperthermophilic ADP-dependent glucokinase from *Thermococcus litoralis* reveal a conserved mechanism for catalysis. *PLoS One 8*, e66687.
(39) Sato, T., and Atomi, H. (2011) Novel metabolic pathways in Archaea. *Curr. Opin. Microbiol. 14*, 307−314.
(40) Chen, L., Spiliotis, E. T., and Roberts, M. F. (1998) Biosynthesis of di-*myo*-inositol-1,1′-phosphate, a novel osmolyte in hyperthermophilic archaea. *J. Bacteriol. 180*, 3785−3792.
(41) Gonçalves, L. G., Borges, N., Serra, F., Fernandes, P. L., Dopazo, H., and Santos, H. (2012) Evolution of the biosynthesis of di-*myo*-inositol phosphate, a marker of adaptation to hot marine environments. *Environ. Microbiol. 14*, 691−701.
(42) Borges, N., Matsumi, R., Imanaka, T., Atomi, H., and Santos, H. (2010) *Thermococcus kodakarensis* mutants deficient in di-*myo*-inositol phosphate use aspartate to cope with heat stress. *J. Bacteriol. 192*, 191−197.
(43) Davis, I. W., Leaver-Fay, A., Chen, V. B., Block, J. N., Kapral, G. J., Wang, X., Murray, L. W., Arendall, W. B., Snoeyink, J., Richardson, J. S., and Richardson, D. C. (2007) MolProbity: all-atom contacts and structure validation for proteins and nucleic acids. *Nucleic Acids Res. 35*, W375−W383.
(44) Chen, V. B., Arendall, W. B., Headd, J. J., Keedy, D. A., Immormino, R. M., Kapral, G. J., Murray, L. W., Richardson, J. S., and Richardson, D. C. (2010) MolProbity: all-atom structure validation for macromolecular crystallography. *Acta Crystallogr., Sect. D 66*, 12−21.

DOI: 10.1021/acs.biochem.5b00296
Biochemistry 2015, 54, 3494−3503